Journal of Neurotrauma

Open camera or QR reader and
scan code to access this article
and other resources online.

ORIGINAL ARTICLE

IMAGING

Application of Delayed Contrast Extravasation Magnetic Resonance Imaging for Depicting Subtle Blood–Brain Barrier Disruption in a Traumatic Brain Injury Model

Sigal Liraz Zaltsman,[1,4,5,*,**] Shirley Sharabi,[2,**] David Guez,[2] Diann Daniels,[2] Itzik Cooper,[1,6,8] Chen Shemesh,[1] Dana Atrakchi,[1] Orly Ravid,[1] Liora Omesi,[1] Daniel Rand,[1] Abigail Livny,[3,8,9] Michal Schnaider Beeri,[1,7] Yael Friedman-Levi,[4] Esther Shohami,[4] Yael Mardor,[2,8,**] and David Last[2,**]

Abstract

The blood–brain barrier (BBB) is composed of brain microvasculature that provides selective transport of solutes from the systemic circulation into the central nervous system to protect the brain and spinal micro-environment. Damage to the BBB in the acute phase after traumatic brain injury (TBI) is recognized as a major underlying mechanism leading to secondary long-term damage. Because of the lack of technological ability to detect subtle BBB disruption (BBBd) in the chronic phase, however, the presence of chronic BBBd is disputable. Thus, the dynamics and course of long-term BBBd post-TBI remains elusive. Thirty C57BL/6 male mice subjected to TBI using our weight drop closed head injury model and 19 naïve controls were scanned by magnetic resonance imaging (MRI) up to 540 days after injury. The BBB maps were calculated from delayed contrast extravasation MRI (DCM) with high spatial resolution and high sensitivity to subtle BBBd, enabling depiction and quantification of BBB permeability. At each time point, 2–6 animals were sacrificed and their brains were extracted, sectioned, and stained for BBB biomarkers including: blood micro-vessel coverage by astrocyte using GFAP, AQP4, ZO-1 gaps, and IgG leakage. We found that DCM provided depiction of subtle yet significant BBBd up to 1.5 years after TBI, with significantly higher sensitivity than standard contrast-enhanced T1-weighted and T2-weighted MRI (BBBd volumes main effect DCM/T1/T2 $p < 0.0001$ $F(2,70) = 107.3$, time point $p < 0.0001$ $F(2,133, 18.66) = 23.53$). In 33% of the cases, both in the acute and chronic stages, there was no detectable enhancement on standard T1-MRI, nor detectable hyper-intensities on T2-MRI, whereas DCM showed significant BBBd volumes. The BBBd values of TBI mice at the chronic stage were found significantly higher compared with age matched naïve animals at 30, 60, and 540 days. The calculated BBB maps were histologically validated by determining significant correlation between the calculated levels of disruption and a diverse set of histopathological parameters obtained from different brain regions, presenting different components of the BBB.

[1]The Joseph Sagol Neuroscience Center, Sheba Medical Center, Tel Hashomer, Israel.
[2]The Advanced Technology Center, Sheba Medical Center, Tel Hashomer, Israel.
[3]Departments of Diagnostic Imaging and Psychiatry, Sheba Medical Center, Ramat Gan, Israel.
[4]Department of Pharmacology, Institute for Drug Research, The Hebrew University, Jerusalem, Israel.
[5]Institutes for Health and Medical Professions, Department of Sports Therapy, Ono Academic College, Kiryat Ono, Israel.
[6]School of Psychology, Reichman University (IDC), Herzliya, Israel.
[7]Department of Psychiatry, The Icahn School of Medicine at Mount Sinai, New York, New York, USA.
[8]Faculty of Medicine, Tel Aviv University, Tel Aviv, Israel.
[9]Sagol School of Neuroscience, Tel Aviv University, Israel.
**These authors made equal contributions to the article.

*Address correspondence to: *Sigal Liraz Zaltsman, PhD, The Joseph Sagol Neuroscience Center, Sheba Medical Center, Tel Hashomer 5265601, Israel* E-mail: Sigal.lirazzaltsman
@sheba.health.gov.il

Cumulative evidence from recent years points to BBBd as a central component of the pathophysiology of TBI. Therefore, it is expected that routine use of highly sensitive non-invasive techniques to measure BBBd, such as DCM with advanced analysis methods, may enhance our understanding of the changes in BBB function after TBI. Application of the DCM technology to other CNS disorders, as well as to normal aging, may shed light on the involvement of chronic subtle BBBd in these conditions.

Introduction

The blood–brain barrier (BBB) describes unique, selective properties of the brain microvasculature that provides selective transport of solutes from the systemic circulation into the central nervous system (CNS) to protect the brain and spinal microenvironment. Multiple structural and functional components, such as the high tight junction (TJ) proteins expression and the close association between brain endothelial cells, pericytes, and astrocytes preserve the integrity of the BBB.[1,2]

Several non-invasive imaging modalities are available for studying BBB disruption (BBBd). Most current approaches track intravenously injected tracers passing from the bloodstream into the brain. In rodents 2-photon microscopy can monitor leakage of fluorescent dyes across the BBB; however, the field of view (FOV) is small, scanning depth is limited, and cannot be translated to humans.[3] Positron emission tomography can assess regional BBBd in humans but repeated scanning for longitudinal assessment is problematic because of ionizing radiation.[3]

The most common technique used for assessing BBBd in traumatic brain injury (TBI) is dynamic contrast-enhanced magnetic resonance imaging (DCE-MRI),[4–7] based on repeated T1-weighted MR images acquired up to 5 min after contrast injection.[8] We have shown previously that higher sensitivity requires longer delays post-contrast injection.[8] In addition, permeability is calculated by applying tracer kinetic models. As a result, different users may rely on different models, which may lead to considerable variability in results.[9,10]

Recently water has been proposed to probe BBB function because it does not diffuse freely across the BBB and it has potential safety benefits. These techniques are not well established yet.[11,12] In addition, most imaging modalities detect significant permeability as seen in brain tumors and multiple sclerosis or in close proximity after acute brain insults, such as stroke and TBI.[6,9,13–16] Non-invasive detection of subtle BBB function changes is challenging and less studied.

TBI, a major health problem with significant, worldwide socioeconomic challenges affecting millions of people, is a complex, dynamic, and heterogeneous pathology.[17,18] TBI results in primary and secondary injury cascades that evolve into chronic brain conditions, including long-term cognitive impairment and reduced quality of life.[19,20] The cognitive impairment frequently persists and may be accompanied by an increased risk of development of neurodegenerative disorders, including Alzheimer disease (AD).[19–22]

Chronic subtle BBBd was suggested in recent years as a major underlying mechanism of cognitive decline,[23,24] specifically post-TBI.[6,25] Identification of subtle BBBd might serve as an early biomarker for chronic consequences after TBI and as a means for monitoring the conversion of acute injury into chronic neurodegenerative disorder. Therefore, there is a great need for non-invasive techniques for the detection and depiction of subtle BBBd. Describing BBBd in TBI using MRI is an emerging field. However, there is a lack of sensitive and quantitative methods, especially in the chronic phase, when BBBd is subtle.[5,9]

Various reports show increased BBB permeability in patients with TBI and animal models by using DCE-MRI, during the acute phase of TBI, when BBBd is significant.[5,26–28] However, reports on long term BBBd based on DCE-MRI are rare, due to the relatively low sensitivity of this method.

The goals of the present study were to assess and histologically validate the application of delayed-contrast extravasation MRI (DCM[8]) to depict and quantify subtle BBB abnormalities with high sensitivity to BBBd and high spatial resolution, in the chronic stage of experimental TBI. To this end, mice were subjected to a closed head injury (CHI) model and scanned with DCM at different time points after injury for up to 540 days. The results were compared with histological biomarkers of BBBd.

Methods
Animals

The study was approved by Sheba Medical Center Animal Ethics Committee and complied with the guidelines of the National Research Council Guide for the care and use of laboratory animals (NIH approval no. OPRR-A5011-01). Male C57BL/6 mice (8–9 weeks old), weighing 20–25 g, were purchased from Envigo (Israel) and maintained under a controlled 12h light/12h dark cycle, with food and water provided *ad libitum*.

Trauma model

Experimental CHI was induced with a modified weight drop device developed in our laboratory.[29,30] Detailed

description of the model and the neurological severity score (NSS) can be found in the Supplementary Material.

Experimental design

Thirty mice were subjected to TBI. They were scanned with MRI 1, 8, 14, 30, 60, 98, 133, and 540 days after injury. At each time point, 3–5 animals were sacrificed and their brains were extracted, sectioned, and stained for BBB biomarkers (Fig. 1A). The BBBd levels, calculated from DCM, were compared with disruption levels calculated from standard MR images and with histological markers. For comparison with normal BBB function, 19 age-matched naïve control mice were scanned with MRI at 30, 60, and 540 days. The BBBd levels, calculated from DCM, were measured in the cortex (same region as in the CHI mice). In addition, several aging mice without trauma (normal aging) were sacrificed at 540 days for evaluation of BBB function by the histological techniques described below.

MRI data acquisition

Mice were scanned under full anesthesia with a 1.5 T GE Optima MRI (Milwaukee, WI), using a standard 8 channel phased array wrist coil. The MR sequences included repeated contrast-enhanced T1-weighted MRI (T1-MRI), acquired up to 30 min post-contrast injection for depicting BBBd (Spin-echo, 12 cm FOV, phase FOV: 0.5, 1 mm slice thickness, echo time/repetition time (TE/TR) = 16/360 msec, 11.9 kHz bandwidth, 256*256 matrix), T2-weighted MRI (T2-MRI) for depicting edema or damage (fast spin echo, 12 cm FOV, phase FOV: 0.5, 1.0 mm slice thickness, TE/TR = 85/3910 ms, 20.83 kHz bandwidth, 256*224 matrix), and gradient echo (GE) for evaluating possible bleeding (10 cm FOV, phase FOV: 0.8, 1.0 mm

slice thickness, TE/TR = 47/124 ms, 15.63 kHz bandwidth, 30 degree flip angle, 256*224 matrix).

Anesthesia was administered via intramuscular injection of 250 μL of 1 mL/kg ketamine and 0.5 mL/kg xylazine. Under anesthesia, a Venflon, connected to a syringe containing 200 μL contrast agent (Gd-DOTA, 0.016 mmol/kg, Dotarem, Guerbert), was inserted in the tail vein. The mice were then placed in the MR scanner. The contrast agent was injected into the tail vein, immediately before the first contrast-enhanced T1-MRI scan.

MRI data analysis

For each mouse, BBB maps were calculated with Matlab (R2014a, Mathworks, Natick, MA). All post-contrast T1-MRIs were coregistered to the first T1-MRI using elastic registration.[31,32] To generate the BBB maps, the first series was subtracted from each of the delayed series. In the generated BBB maps, contrast clearness (negative signal) is colored blue, contrast accumulation (positive signal) is colored red, and No change in signal (when the contrast does not leak into the brain) is colored green in the maps. The BBB maps were generated for each time point post-contrast injection.

To calculate the lesion volume and BBBd volumes and intensities, regions of interest (ROIs) were plotted over all brain slices affected by the insults (Fig. 1B). For the lesion volume, ROIs were plotted over hyperintense regions on T2-MRIs and enhancing regions on the first post-contrast T1-MRI (unless undetected). For BBBd volumes and intensities, ROIs were plotted over the red regions in the 30 min BBB maps.

Next, the average intensity of the BBBd ROI, normalized to the first time point, was plotted as a function of time post-contrast injection for each mouse at each time point post-TBI. The plot was fitted to an exponential

FIG. 1. Experimental design and schematic illustration of the regions of interest (ROIs) used for histological analysis. A total of 30 traumatic brain injury (TBI) and 19 sham age matched mice were included in the study. (**A**) A TBI was induced at day 0. The X axis represents time from TBI. The colored squares represent the procedure performed at each time point, according to the legend on the right panel. (**B**) On the left, a three-dimensional illustration of a mouse brain showing the lesion area in the left hemisphere and the magnetic resonance imaging (MRI) coronal slices. Second panel: illustrations of T2-weighted MRI slices of a mouse head (dark gray) and brain (light gray), corresponding to specific coronal MRI slices where the lesion (bright area in the left hemisphere) was observed. Third panel: representative blood–brain barrier (BBB) maps from the same slices as the T2 illustrations 4 days post-injury. The intact brain, colored green, is surrounded by the head muscles (blue). Contrast accumulation results in a positive signal, appearing red in the maps. On the right, schematic of the ROIs used for histological analysis. The coronal sections represent the slices affected by the primary insult induced by the weight drop device. Three ROIs were captured from the ipsi- (directly injured cortex) and contralateral hemisphere, marked in roman numerals I–IIIi (ipsilateral) and I–III.c (contralateral). Region Ii, located laterally and adjacent to the lesion is the cingulate gyrus (CG), which is the area most affected directly by the impact. Region IIi, inside the lesion area, is referred to as the lesioned cortex (LC). Region IIIi, the parietal cortex (PC), is located medial and is relatively remote from the lesion, and not directly affected by the insult. Regions I–IIIc are the corresponding regions in the contralateral hemisphere. Representative hematoxylin and eosin (H&E)-stained samples from the three ROIs (x200) from both hemispheres at the acute stage are shown in the bottom line. CHI, closed head injury.

function (Equation 1) with four free parameters (X_1-X_4) by using an algorithm based on golden section search and parabolic interpolation, available under Matlab.[33,34] Goodness of fit was established according to the coefficient of determination (r^2), and the maximum fit value was extracted and used as the maximal normalized disruption intensity, indicating the severity of disruption. To avoid random effects from MR signal noise, $r^2 > 0.85$ was used as the minimum inclusion threshold in the analysis. The same procedure was applied to the naïve group of mice.

$$X_1 \cdot \left(e^{\left(-\frac{t}{X_2} \right)} + e^{\left(-\frac{t}{X_3} \right)} \right) + X_4 \qquad \text{Equation (1)}$$

Tissue preparation for analysis

Mice were sacrificed after the MRI scan at each time point as described in the study design (Fig. 1). Brains were removed quickly, washed with saline, frozen on dry ice, and stored at -80°C until analyzed. Several consecutive series of sections ($10\,\mu m$) were made at a cutting temperature of -19°C (Leica cm1850 Leica Biosystems, Nussloch, Germany) from the prefrontal cortex to the cerebellum and thaw-mounted onto coated glass slides. These serial sections were used for H&E and immunofluorescence staining.

Immunofluorescence staining

Consecutive serial sections were used for Immunofluorescence staining with the following antibodies:
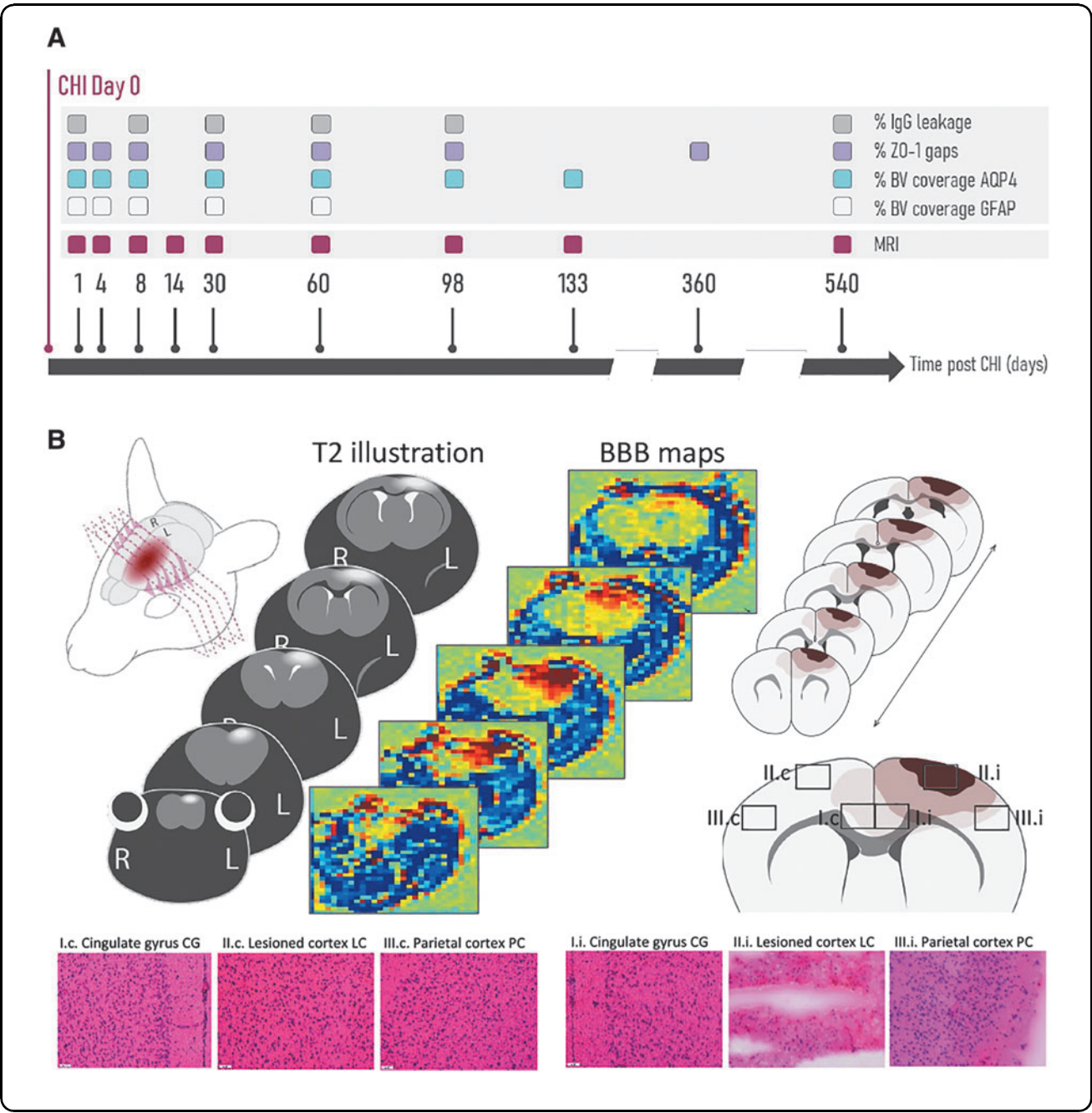
lectin-FITC (1:400 Zotal FL-1171), Claudine 5 (anti rabbit 1:500 sc-28670), GFAP (anti goat 1:1000 abcam ab53554), AQP4 (H-80 anti-rabbit 1:400 Santa Cruz sc-20812), and zonula occludens 1 (ZO-1, anti rabbit 1:200 Invitrogen 61-7300).

Briefly, after fixation in 4% paraformaldehyde for 10 min, the sections were washed with phosphate buffered saline (PBS) containing 0.1% triton (PBST) $3\times$ 10 min, blocked (10% normal donkey serum in PBST) for 1h at room temperature (RT), and incubated overnight at 4°C in the presence of primary antibodies. The following day, the sections were washed with PBST 3×10 min and incubated with the corresponding secondary antibodies: donkey anti-rabbit CY3 1:1000 (Jackson 711-165-152), Alexia flour 488, anti-rabbit 1:1000 (Jackson 711-545-15200), donkey anti-goat CY3 1:500 (Jackson 705-165-147) in 2% donkey serum for 1h at RT, rewashed with PBST 3 times for 10 min, stained with Hoechst (1:2000) for 2 min and washed with PBS for 5 min. Finally, the sections were air-dried, mounted on coverslips, and sealed with fluoromount (Sigma F4680, Israel).

All steps involving fluorescence were performed in a slightly darkened room. Each slice was costained with lectin (general blood vessel marker) and one of the other markers mentioned above: AQP4 and GFAP for blood vessels (BV) coverage analysis, ZO-1 for TJ gap analysis, and immunoglobulin G (IgG) for leakage analysis. The immunostained slices were examined under a fluorescence microscope.

Immunofluorescence analysis

Histological analyses were performed by a blinded examiner. The images were captured under identical optical parameters and analyzed with ImageJ (National Institutes of Health, Bethesda, MD) using automatic scripts when possible to avoid subjective decisions. Three ROIs were identified for each hemisphere (ipsi- and contralateral to the injury): (1) Lesioned cortex (LC), inside and surrounding the lesion area, (2) cingulate gyrus (CG), located laterally and adjacent to the LC, the region most directly affected by the insult, and (3) parietal cortex (PC), located medially and remote from the lesion namely on the same slices but not directly affected by the insult (Fig. 1).

For quantification of ZO-1 gaps, the lengths of the 11-17 BVs were measured in each region from each side (ipsilateral/contralateral) for each time point from 3–8 different images captured from at least four serial sections spaced 150 μm apart, representing the whole ROI. Sham animals (540 days post-TBI) were used to measure ZO-1 gaps in normal aging animals. The ZO-1 gap length is presented as the percentage (%) of the whole TJ staining, calculated according to the lectin marker.[35]

For microvessel coverage, two markers were used: GFAP labeling all astrocyte cells including the end-feet and AQP-4, which is expressed mainly at the astrocyte end-feet. The microvessel coverage measured with GFAP was calculated at the ipsilateral hemisphere, from days 1–98 post-injury. We sampled brains from six time points after injury (days 1, 4, 8, and 1, 2, and 3.3 months) in three regions: LC, CG, and PC. Because the GFAP antibody used for staining is not sensitive enough to mark astrocytes in the contralateral hemisphere (probably because the astrocytes are only partially activated), only the injured hemisphere was measured.

Microvessel coverage immune-stained with anti AQP-4 antibody was measured in both hemispheres: the lesioned/ipsilateral hemisphere and the non-injured/contralateral hemisphere, from 1– 540 days post-injury.

Brains were sampled from eight time points after the injury (days 1, 4, 8, and 1, 2, 3.3, 4.5, and 18 months) in three regions (similar to those measured for GFAP: LC, CG, and PC). For calculating BVs coverage by astrocytic end-feet (AQP4 or GFAP), five images of CG and PC were captured from at least four serial sections, spaced 150 μm apart, from each hemisphere (ipsi- and contralateral) at each time point, representing the whole ROI.

Because the LC region showed larger variability, at least 10 images of that region were captured from five serial sections spaced 150 μm apart at each time point. The images were converted into eight bits, and a threshold was set for the lectin staining representing the BV. The same threshold was used for all the images.

Next, pixel by pixel analysis was performed automatically to measure colocalization with the red signal representing AQP4 or GFAP. Percent coverage was calculated by dividing the sum of the colocalization signal from the total lectin staining. Sham animals (540 days) were used to measure AQP4 coverage in normal aging animals. For IgG leakage analysis, images were captured from the ipsi- and contralateral LC regions only for the first five time points after injury: 1, 8, 60, 98, and 133 days. The intensity of the IgG outside the BV was measured for each image.

Figure 1A summarizes all the immunofluorescence analysis according to day from injury. Figure 1B (right panel) illustrates the various regions that were captured from different serial sections.

Statistical analysis

The results are expressed as mean $\pm$ standard deviations (SD) for all experiments. For two groups comparisons, statistical significance was determined according to the unpaired Student t test. For multiple groups comparison at different time points, two-way analysis of variance (ANOVA) or a mixed effects model was used with appropriate *post hoc* analysis using Prism 9.3.1 software

(GraphPad Software, La Jolla, San Diego, CA). A probability value of $p < 0.05$ was considered significant.

To determine sensitivity of BBB maps at all time points, compared with conventional contrast enhanced T1-MRI, a mixed effects model was used. The within-subjects t test was used to determine the significance at each time point. To describe BBBd intensity and volume over time, exponential decay function was fitted to the data according to the least square method. Pearson correlation was used to assess the correlation between MRI-based BBBd intensity and histological-based BBBd parameters in different ROIs. All data were tested for normality using the Shapiro-Wilk test of normality and were found normally distributed.

Results

Delayed-contrast MRI is significantly more sensitive to BBBd than standard MRI

To compare the sensitivity of DCM with that of standard MRI, the BBBd ROI volumes calculated from the BBB maps were compared with the enhancing lesion volumes calculated from the post-contrast T1-MRIs. Volume comparison with hyperintense ROIs calculated from T2-MRIs, representing edema or damage, was also performed. The average volumes of these ROIs as a function of time post-injury are shown in Figure 2.

Significant main effects of BBBd volumes were found in the mixed-effects model for the measurement (DCM / T1/T2) $p < 0.0001$ F(2,70) = 107.3, time point $p < 0.0001$ F(2,133, 18.66) = 23.53 and interaction of time point versus measurement $p < 0.0001$ F(16,70) = 5.40. In all but one time point (day 98), BBBd volumes calculated from DCM were significantly larger than the enhancing volumes calculated from standard post-contrast T1-MRIs. In 33% of the cases, both in the acute and chronic stages, there was no detectable enhancement on standard T1-MRI, nor detectable hyperintensities on T2-MRI, whereas DCM showed significant BBBd volumes (Fig. 2).

The average disruption volumes and normalized intensities were largest immediately after the injury ($0.025 \pm 0.006 \, \text{mm}^3$ and $1.23 \pm 0.04\%$, respectively), the lowest values appearing on days 30 and 60 ($0.005 \pm 0.002 \, \text{mm}^3$ and $1.13 \pm 0.02\%$ on day 30; $0.003 \pm 0.001 \, \text{mm}^3$ and $1.14\% \pm 0.026\%$ on day 60). From that time on, both the volumes and the normalized intensities remained stable up to 540 days post-injury, suggesting persistent BBBd. Further, we found that BBBd volumes decreased significantly by day 8 (from $0.025 \pm 0.006 \, \text{mm}^3$ to $0.012 \pm 0.00^3 \, \text{mm}3$, $p < 0.0091$), suggesting partial BBB function recovery within the acute stage.

To confirm that the chronic BBBd values represent chronic disruption, we compared them with normal BBB function, calculated from ROIs in the cortex of age-matched naïve animals at 30, 60, and 540 days.

The results showed that the normalized BBBd intensities of the control mice were significantly lower than those of the TBI mice, with values of 1.03 ± 0.06, 1.002 ± 0.009, 1.022 ± 0.014 at 30, 60, and 540 days, respectively. These results imply that BBB malfunction persists up to 540 days after the injury (Fig. 3).

Blood vessel coverage by astrocytic end-feet is significantly reduced in the acute stage, with partial recovery over time

Percent microvessel coverage was calculated in the LC, CG, and PC regions (Fig. 1B). The microvessel coverage measured with GFAP was calculated for the ipsilateral hemisphere from days 1–98 post-injury. Microvessel coverage measured with AQP-4 was calculated for both hemispheres from days 1-540 post-injury.

Vessel coverage measured by GFAP immunostaining colocalized with lectin. Microvessel coverage was calculated for each region (LC, CG, PC) of each mouse at each time point (Fig. 4E). The coverage was low immediately post-injury (LC: $35.17\% \pm 24.5$, CG: $60.42\% \pm 14.52$, PC: $65.06\% \pm 5.5\%$), but increased, suggesting improvement over time (significant main effect with time from the initial injury with one-way ANOVA, LC: $p < 0.0023$, CG: $p < 0.2$, PC: $p < 0.3$). The initially low coverage after injury indicates partially bare vessels, characteristic of severe BBBd,[36] with significant improvement up to 98 days following injury.

There were no significant differences between the LC, CG, and PC regions, although the regions adjacent to the lesion showed a more severe trend (Fig. 4E). The PC region, located remotely from the site of injury, revealed relatively low initial coverage ($65.06 \pm 5.5\%$), suggesting it was affected as well.

Because no significant differences were found between the LC, CG, and PC regions (main effect for region, two-way ANOVA, F (2, 43) = 2.489, $p = 0.09$), we combined the three regions and referred to the combined region as the ipsilateral cortex (Fig. 4A–D), similarly to the MRI region. Like the MRI results, there was a significant increase in vessel coverage between day 1 and day 30 post-injury ($55.10 \pm 24.59\%$, $74.01 \pm 9.30\%$, $p < 0.049$).

Vessel coverage measured by AQP-4 immunostaining colocalized with lectin. AQP-4 is expressed on astrocyte end-feet covering brain endothelial cells and is, therefore, considered more sensitive than GFAP.[36] Vessel coverage was measured for up to 540 days post-injury and showed more sensitive but similar trends to those observed with GFAP staining. Coverage was low immediately post-injury (ipsilateral: LC: $6.03 \pm 3.17\%$, CG: $17.84 \pm 7.84\%$, PC: $6.46 \pm 5.80\%$; contralateral: LC: $26.93 \pm 11.29\%$, CG: $28.98 \pm 10.87\%$, PC: $44.24 \pm 25.84\%$) but significantly increasing, suggesting
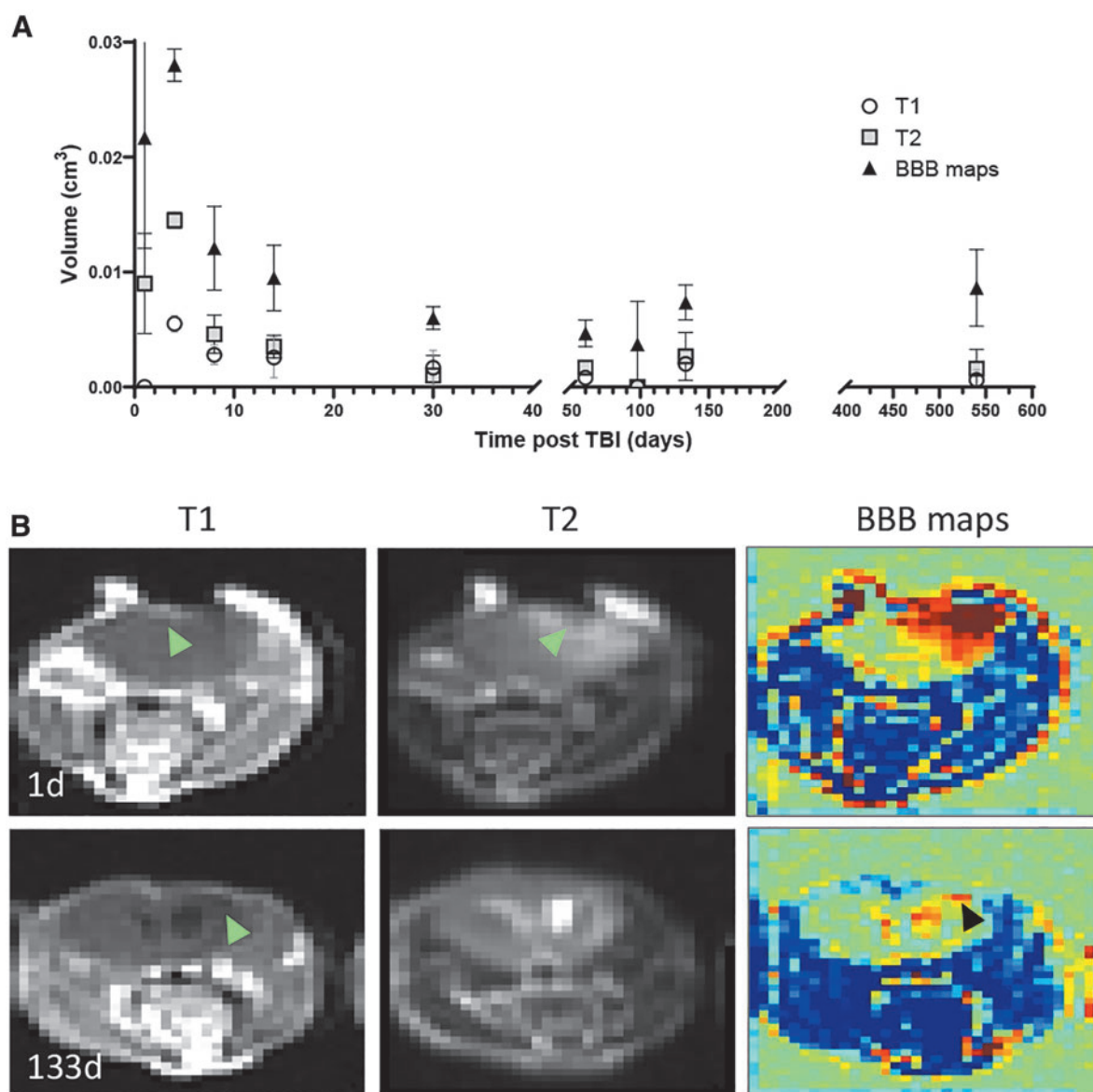
FIG. 2. Delayed contrast extravasation magnetic resonance imaging (DCM) is significantly more sensitive to blood–brain barrier (BBB) disruption than standard magnetic resonance imaging (MRI). **(A)** Average region of interest (ROI) volumes calculated for each time point from DCM, T1-MRI, and T2-MRI. The p values per time point: day 1: DCM vs. T1: 0.05, DCM vs. T2: 0.1 ns; day 4: DCM vs. T1: 0.009, DCM vs. T2: 0.01; day 8: DCM vs. T1: 0.003, DCM vs. T2: 0.007; day 14: DCM vs. T1: 0.0009, DCM vs. T2: 0.002; day 30: DCM vs. T1 and T2: 0.01; day 60: DCM vs. T1 and T2: 0.02; day 98: DCM vs. T1 and T2: 0.2 ns; day 133: DCM vs. T1: 0.02, DCM vs. T2: 0.03; day 540: DCM vs. T1: 0.004, DCM vs. T2: 0.005. **(B)** Representative T1-MRIs, T2-MRIs, and BBB maps acquired 1 and 133 days after injury. The arrowheads point to the affected lesion cortex. It can be seen that subtle yet significant BBBd was detected in mice up to 540 days post-injury. TBI. Traumatic brain injury.

improvement, over time (significant main effect for the time elapsed from the initial injury, one-way ANOVA, ipsilateral LC: $p < 0.0001$, CG: $p < 0.0017$, PC: $p < 0.0013$; contralateral: LC: $p < 0.06$, CG: $p < 0.0001$, PC: $p < 0.6$). This initially low coverage after injury indi-

cating partially bare vessels, characteristic of severe BBBd,[36] was significantly improved in the course of the 540 day follow-up (Fig. 4J).

There were no significant differences between the LC, CG, and PC regions (main effect for region by two-way
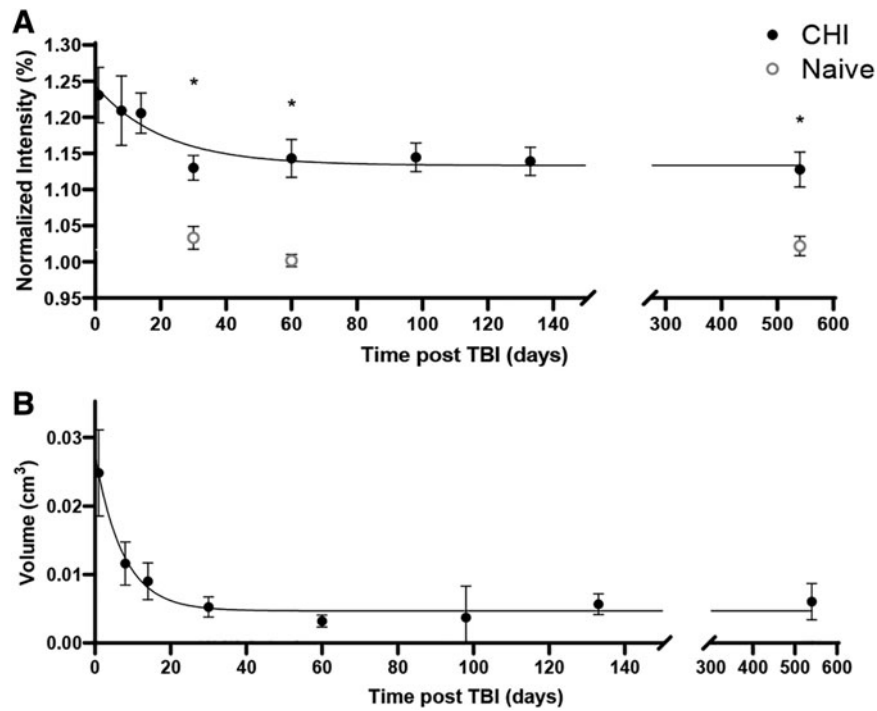
FIG. 3. Delayed contrast extravasation magnetic resonance imaging (DCM)-based blood–brain barrier (BBB) disruption volumes and intensities in mice post-traumatic brain injury (TBI). (**A**) Average normalized intensities as function of time post- injury ($n=3$– 5 animals/time point): day 1: 1.23%$\pm$0.037; day 8: 01.21%$\pm$0.048; day 14: 1.21%$\pm$0.028; day 30: 1.13%$\pm$0.017; day 60: 1.14%$\pm$0.026; day 98: 1.15%$\pm$0.020; day 133: 1.14%$\pm$0.019; day 540: 1.13%$\pm$0.024. Average normalized intensities at 30, 60, and 540 days for naive animals: day 30: 1.033%$\pm$0.016; day 60: 1.002%$\pm$0.009; day 540: 1.022%$\pm$0.014. (**B**) Average BBBd volume as function of time post-injury in mm^3: day 1: 0.025$\pm$0.006; day 8: 0.012$\pm$0.003; day 14: 0.009$\pm$0.003; day 30: 0.005$\pm$0.002; day 60: 0.003$\pm$0.001; day 98: 0.004$\pm$0.005; day 133: 0.006$\pm$0.002; day 540: 0.006$\pm$0.003.

FIG. 4. Blood vessel (BV) coverage by astrocytic end-feet. Immunofluorescence staining of microvascular endothelium (claudin-5, green) coverage by astrocytes (GFAP, red). (**A–C**) representative images from the ipsilateral lesion cortex (LC) region on days 1, 30, and 60, respectively. Arrowheads show colocalization of GFAP and BVs. The yellow signal indicates high BV coverage by the astrocytes, the green signal indicates bare vessels not covered by astrocytes, reflecting BBB disruption. Scale bar, 100 μm. (**D**) Percent GFAP coverage as a function of time post-TBI for all three ipsilateral regions of interest (ROIs) (LC, CG, and PC). (**F,G**) Representative images of immunofluorescence staining of microvascular endothelium (lectin, green) coverage by astrocyte end-feet (AQP4, red) from ipsi- and contralateral LC on day 1 after injury. Scale bar, 50 μm. (**H**): High magnification of vessels from ipsi- and lateral LC 1 day after injury showing highly affected vessels with no coverage at the ipsilateral cortex versus covered vessels at the contralateral cortex. The diameter of the vessel lumen ($\leq$ 10 μm) indicates that microvessels were included and not regular/larger vessels. (**I**) Percent AQP4 coverage as a function of time for all three ROIs (LC, CG, and PC) from the ipsi- and contralateral hemispheres. Significant main effects for time elapsed post-injury $p<0.0001$) and for side (ipsilateral versus contralateral, $p<0.0003$). (**E, J**) Heat map spectrum of values: red colors represent low coverage values (BBB disruption), green colors indicate high coverage values (E-GFAP, I-AQP4). Rows represent different time points, the columns represent different ROIs, the X axis represents distance from injury. The map shows the increase of coverage over time (the upper rows appear green, indicating high coverage long after injury) and the differences between the ROIs, although they were not statistically significant. Note: region I at the contralateral hemisphere refers to the cortical region corresponding to the LC in the contralateral hemisphere.

ANOVA, ipsilateral: $F_{(2, 10)} = 2.24$, $p = 0.16$, contralateral: $F_{(2, 12)} = 2.044$, $p = 0.17$), although the regions adjacent to the lesion showed a more severe trend (Fig. 4I). Because no significant differences were found between the LC, CG, and PC regions, we combined the three

regions and referred to the combined region as the ipsilateral cortex (Fig. 4 E–I), similarly to the MRI region.

Like the MRI results, there was a significant increase in vessel coverage between day 1 and day 8 ($10.08 \pm 7.72\%$, 23.40 ± 8.38, $p < 0.0018$) and between day 1 and
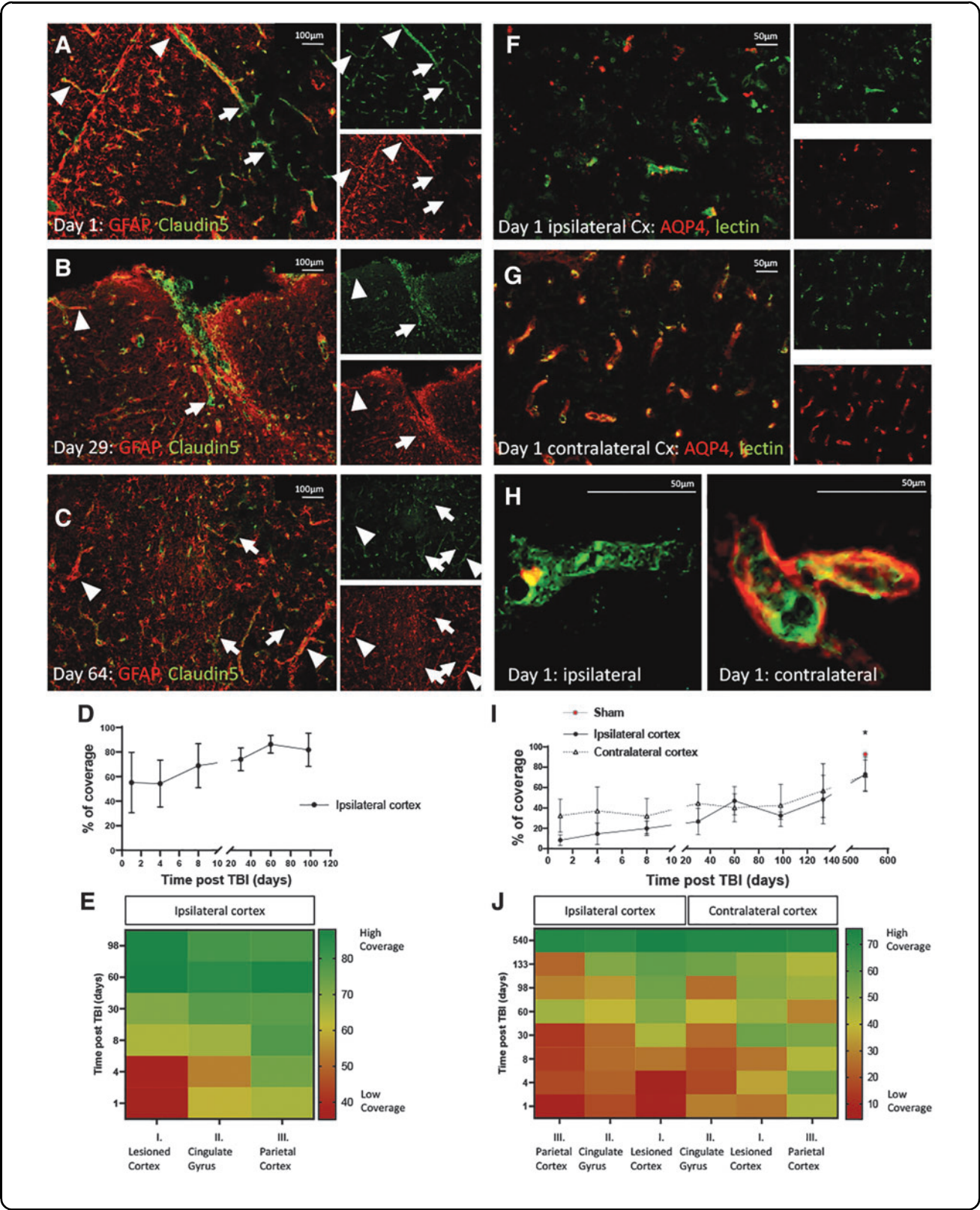
day 30 post-injury ($10.08 \pm 7.72\%$, $27.24 \pm 15.10\%$, $p < 0.0051$). Unlike the MRI results, this effect continued, with an additional significant increase between days 60–540 post-injury ($46.92 \pm 14.03\%$, $73.07 \pm 16.97\%$, $p < 0.002$).

All the contralateral regions, located remotely from the injury site, showed low initial coverage (~ 27–44% in comparison with the aged controls, 92%, Fig. 4H), suggesting they were affected as well. Further, the recovery of the ipsilateral hemisphere was significantly faster than that of the contralateral hemisphere (Fig. 4H), as reflected by the significant main effects for the time elapsed from the initial injury (two-way ANOVA, LC: F (2.316, 10.590) = 10.34, $p = 0.0026$, CG: F (1.510, 5.826) = 16.95, $p = 0.0047$; PC: F (1.387, 4.558) = 3.558, $p = 0.12$).

To confirm that the microvessel coverage values observed at 540 days represent persistent disruption, we compared them with normal BBB function, calculated for matched aged naïve mice. The results showed that microvessel coverage of the control mice ($92.67 \pm 4.12\%$) was significantly higher than that of the TBI mice (ipsilateral/contralateral: $73.07 \pm 16.97/72.24 \pm 15.02\%$, $p < 0.0001$ for both). These results imply that BBB malfunction persists up to 540 days after injury.

The percentage of ZO-1 gaps was high in the acute stage, with partial recovery over time

The percentage of gaps was high immediately post-injury (ipsilateral: LC: $48.71\% \pm 9.59\%$, CG: $59.43\% \pm 8.70\%$ and PC: $48.77\% \pm 5.87\%$; contralateral: LC: $50.14 \pm 8.03\%$, CG: $51.04 \pm 4.17\%$, PC: $50.27 \pm 6.17\%$), with a significant d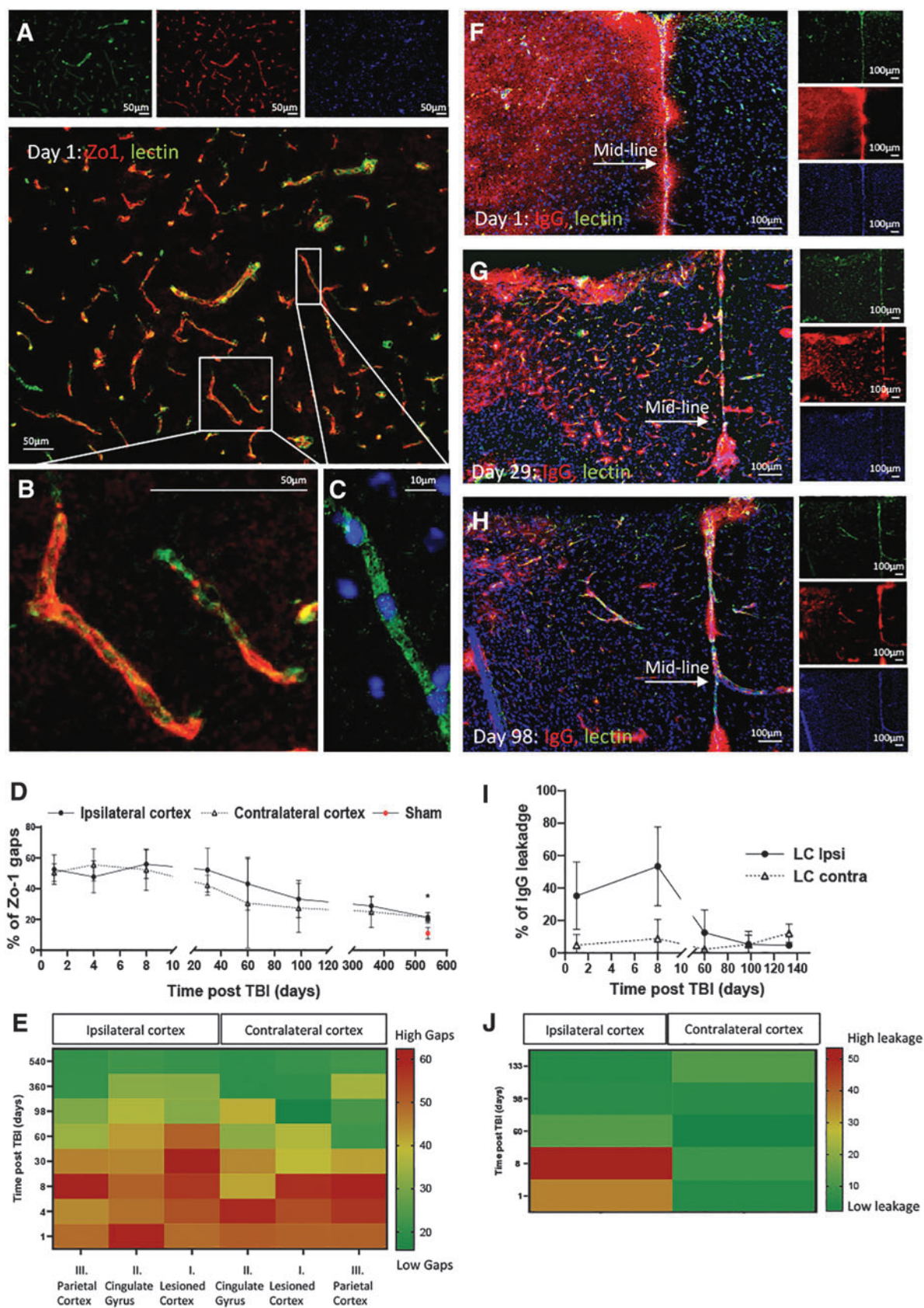ecrease, suggesting improvement, over time (significant main effect for the time elapsed from the initial injury according to one-way ANOVA, ipsilateral LC: $p < 0.0004$, CG: $p < 0.0003$, PC: $p < 0.0001$; contralateral: LC: $p < 0.0001$, CG: $p < 0.0008$, PC: $p < 0.0001$). This initially high gap percentage after injury indicated poor integrity of the TJ, characteristic of severe BBBd,[35] with significant improvement throughout the 540 day follow-up (Fig. 5E).

There were no significant differences between the LC, CG, and PC regions (main effect for region by two-way ANOVA, ipsilateral: F (1, 59) = 0.137, $p = 0.71$, contralateral: F (1, 15) = 0.010, $p = 0.92$). Because no significant differences were found between the LC, CG, and PC regions, we combined the three regions and referred to them as the ipsilateral cortex (Fig. 5D, 5E). Unlike the MRI and vessel coverage findings, there was no significant improvement in the percentage of ZO-1 gaps between day 1 and day 8 ($p < 0.31$) or between day 1 and day 30 post-injury ($p < 0.95$). Unlike the MRI results, recovery was significant between day 60 and day 540 post-injury ($43.16 \pm 17.20\%$, $21.36 \pm 2.79\%$, $p < 0.003$).

The contralateral regions, located remotely from the injury site, showed a high initial percentage gaps, similar to those of the ipsilateral regions (~ 50–51%, Fig, 5D), suggesting they were significantly affected as well. The recovery of the ipsilateral hemisphere was similar to that of the contralateral hemisphere (Fig. 5D).

To confirm that the percentage of ZO-1 gaps found at 540 days represents persistent disruption, we compared them with those of normal BBB function, calculated for matched age naïve mice. The results showed that the percentage of ZO-1 gaps of the control mice ($10.93 \pm 3.66\%$) was significantly lower than that of the TBI mice

FIG. 5. Blood vessel (BV) integrity: tight junction protein ZO-1 and IgG leakage. Immunofluorescence staining of microvascular endothelium (lectin, green) with tight junction protein ZO-1 (ZO-1, red). (**A, B**) Representative images from ipsilateral lesioned cortex (LC) from day 1, low and higher magnification, scale bar 50 μm. The images represent the variability in BV integrity. Two BVs from the ipsilateral cortex of injured mice are presented in B: whereas the left vessel is fully covered by ZO-1, implicating intact blood–brain barrier, the right vessel shows discontinuous, less regular distribution of ZO-1. (**C**) High resolution of mmunofluorescence staining of microvascular endothelium (lectin, green) with nucleus (DAPI, blue) illustrating the diameter of the BVs included in the analysis, indicating that they are microvascular and not larger vessels. (**D**) Average combined percentage of ZO-1 gaps as a function of time of all three regions of interest (ROIs, LC, CG, and PC) of the ipsi- and contralateral hemispheres. Significant main effects for time post-injury (two-way analysis of variance, ipsilateral: F (2.81,23.70) = 9.70, $p = 0.0003$, contralateral: F (1.88,12.68) = 15.19, $p = 0.0005$)). (**E**) Heat map representing ROI differences. The rows represent time points from injury. The columns represent the three regions (LC, CG, and PC from left to right). Heat map spectrum of values (red colors represents high values (disruption, green colors indicate low gap values). The map clearly shows a decrease in gaps over time and the differences between the ROIs. (**F–H**) Immunofluorescence staining of microvascular endothelium (lectin, green) with IgG (IgG, red) showing leakage of this large molecule from the BVs into the brain parenchyma. Representative images from midline cortex showing the ipsi- and contralateral cortices from days 1, 30, and 98 after injuries. Nuclei from all the cells were labeled with Hoechst stain (blue). (**I**) Percentage of IgG leakage as a function of time for the LC region of the ipsi- and contralateral hemispheres. (**J**) Heat map of IgG leakage in the LC region of the ipsi- and contralateral hemispheres.

(ipsilateral/contralateral: $21.36 \pm 2.79/22.07 \pm 4.69\%$, $p < 0.0001$ for both). This implies that BBB malfunction persists up to 540 days after the injury.

High levels of IgG leakage into the perilesional cortical parenchyma, representing BBBd, were detected at acute stages

The leakage, measured for up to 133 days, was high immediately post-injury in the ipsilateral hemisphere (ipsilateral: $35.17\% \pm 20.82\%$; contralateral: $4.82 \pm 6.45\%$) with significant decrease, suggesting improvement, over time (significant main effect for the time elapsed from the initial injury, one-way ANOVA, ipsilateral $p < 0.0004$; contralateral: $p < 0.0001$). This initially high IgG leakage after injury indicating high permeability, characteristic of severe BBBd,[37] was followed by significant improvement throughout the 133 day follow-up (Fig. 5E).

The IgG in the ipsilateral hemisphere trended to recover between days 1 and 133 ($35.17 \pm 20.82\%$, $4.69 \pm 1.65\%$, $p < 0.06$). Unlike the vessel coverage levels and the percentage of ZO-1 gaps, the contralateral region showed low initial leakage and, therefore, no significant recovery was evident (reaching $12.14 \pm 5.72\%$, Fig, 5D).

Significant correlation between MRI-based BBBd intensity and histological-based BBBd parameters

The correlation between the normalized BBBd intensity, calculated from DCM, and each of the histological parameters measured in the different regions (Fig. 6) was determined according to Pearson correlation. The BBBd calculated from DCM was significantly correlated with the percentage of vessel coverage measure with GFAP and AQP4 at the ipsilateral LC and CG regions (these regions were adjacent to the injury and directly influenced by the cortical weight drop impact): BBBd vs. % GFAP coverage: $r^2 = 0.87$, $p < 0.0065$, $r^2 = 0.962$, $p < 0.0006$, for LC and CG, respectively; BBBd vs. % AQP4 coverage: $r^2 = 0.879$, $p < 0.0006$, $r^2 = 0.59$, $p < 0.04$ for LC and CG, respectively; BBBd vs. % of ZO-1 gaps: $r^2 = 0.56$, $p < 0.05$, $r^2 = 0.78$ $p = 0.04$, for LC and CG, respectively; and BBBd vs. % of IgG leakage: $r^2 = 0.76$, $p < 0.05$.

Thus, an increase in BBBd, reflected by an increase in normalized DCM intensity, was accompanied by decreased vessel coverage by astrocyte end feed, an increased percentage of ZO-1 gaps, and increased levels of IgG extravasation.

Discussion

BBBd is a well-known consequence of TBI in the acute stage and is associated with poor physical, emotional, and cognitive outcomes.[38] Recently, some evidence of more persistent and chronic BBBd emerged. Extravasation of the serum protein fibrinogen, and IgG, both markers for BBBd, were observed in the brains of patients who died in the acute phase after TBI, as well as in those who survived at least one year.[39] Early restoration of BBB integrity was suggested to help prevent the sequelae of other long-term comorbidities associated with TBI, such as post-traumatic epilepsy and neurodegenerative diseases.[38–40]

At present, knowledge regarding BBBd after TBI is mainly based on post-mortem investigations in humans and experimental animals. Despite the large body of evidence for the TBI long-term repercussions, however, there is a critical lack of reliable methods addressing BBBd *in vivo,* impeding dynamic BBBd assessment in the same individual over time and necessary for evaluating both the acute and chronic phases of TBI.

Therefore, enhancing our knowledge of temporal BBB dynamics is required and non-invasive imaging methods, highly sensitive to subtle BBB changes/disruption, that enable to longitudinally explore BBB function, are needed. The application of MRI to the quantification of BBB abnormalities is an emerging field.[6] There is a lack of quantitative and sensitive methods, however, especially in the chronic phase because of the challenges encountered at subtle levels of BBBd.

So far, DCE MRI is the most common technique used for this purpose. The DCE is a perfusion technique from which quantitative parameters reflecting microcirculatory structure and function can be derived. Of those, Ktrans (the volume transfer constant between the plasma and the extravascular extracellular space) is most commonly used for BBBd quantification after TBI.[6,41]

Reports on the utility of DCE-based parameters as imaging biomarkers of BBBd in TBI are scarce.[42] Recently, BBBd in the periventricular regions in 10 of 19 rugby players, observed by acquiring DCE pre- and post-season, supported the notion of long-term BBBd in mild TBI. Similarly, modified prolonged DCE-MRI scans revealed the BBBd in a subset of amateur American football players exposed to repeated mild TBI.[27] The increased permeability persisted for months, as seen in players who were scanned both on/off-season for two consecutive seasons of play and practice.

Regional DCE analysis has shown that in concussed football players or mixed martial arts athletes, the number of regions with BBBd (>2 SD of controls) deviated from the normal distribution, but not in age-matched healthy controls. Although group comparison showed no differences in the overall BBBd volume in players compared with controls, up to 35% of the players exhibited shared brain regions with BBBd. Importantly, BBBd was found in a few players ($n = 4$) weeks and months after the last concussion. Recently, however, it has been recognized that the sensitivity of DCE to subtle BBBd is low.[43]
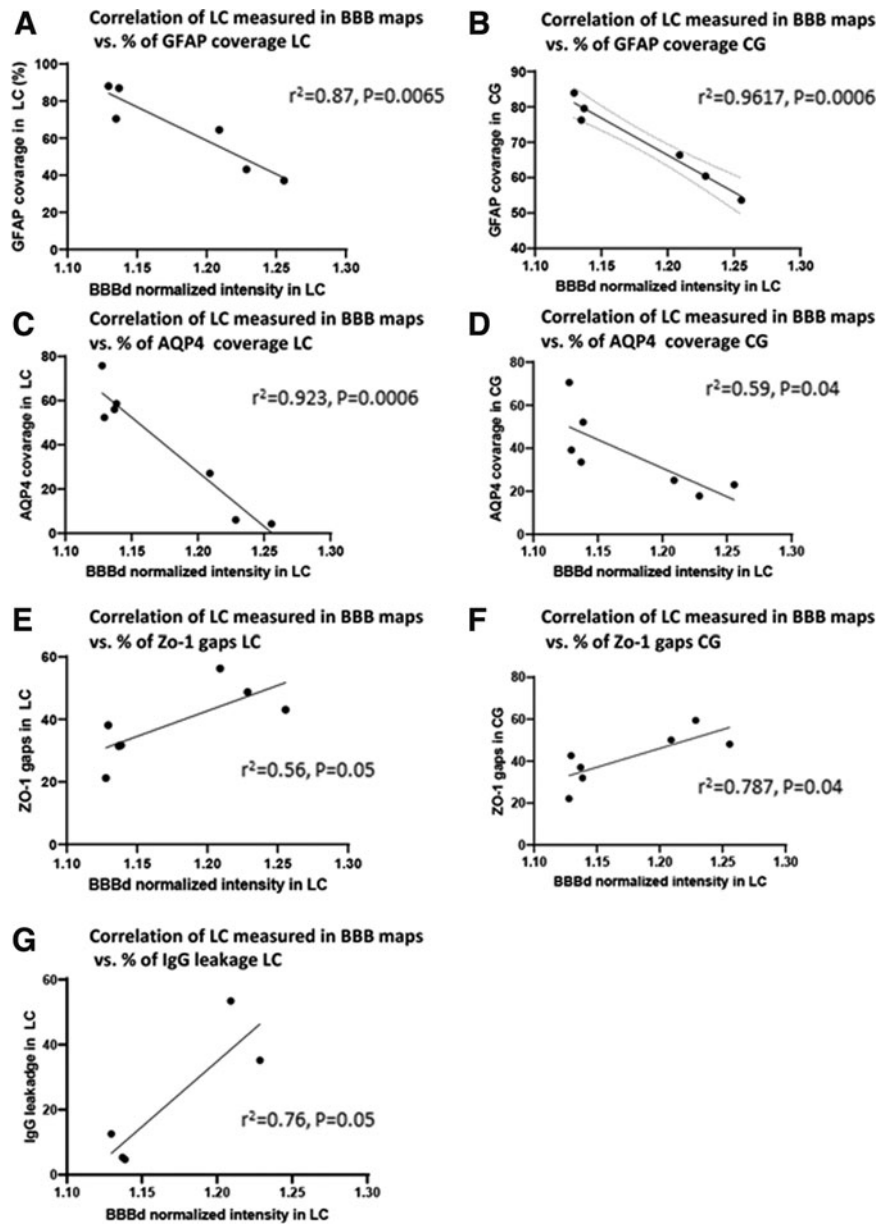
FIG. 6. The correlation between magnetic resonance imaging (MRI)-based blood–brain barrier disruption (BBBd) intensity and histological-based BBB parameters. Correlations were determined between the normalized BBBd intensity, calculated from Delayed contrast extravasation magnetic resonance imaging (DCM) and various histological parameters measured in the different regions. The percentage of GFAP coverage in the lesioned cortex (LC) and cingulate gyrus (CG) was found to be significantly correlated with the MRI-based intensity of BBBd. In both regions, affected directly by the cortical weight drop impact, the correlations were significantly negative: $r^2 = 0.87$, $p < 0.0065$ for LC (**A**) and $r^2 = 0.962$, $p < 0.0006$ for CG (**B**). Thus, the higher the intensity of the BBBd, the lower the percentage of GFAP coverage. The percentage of AQP4 coverage in both the LC and CG regions was found to be significantly correlated with the MRI-based intensity of BBBd. Although the two comparisons showed significant statistical significance, a stronger negative correlation was measured in the LC region (LC: $r^2 = 0.923$, $p < 0.0006$ [**C**], CG: $r^2 = 0.59$, $p < 0.04$ [**D**]). The percentage of ZO-1 gaps, representing the tight junctions of endothelial cells, in the LC and CG was found to be significantly correlated with the MRI-based intensity of BBBd. In both regions significant positive correlations were found, with values of $r^2 = 0.56$, $p < 0.05$, LC (**E**) and $r^2 = 0.78$ $p < 0.04$, CG (**F**). Significant correlation was also found between the percent of IgG leakage into brain parenchyma and the MRI-based intensity of BBBd: $r^2 = 0.76$, $p < 0.05$ (**G**).

These data suggest that there is enduring BBBd after TBI. Advancing methodologies for assessment of subtle changes in BBB function are essential for shedding light on BBBd as a potential major underlying mechanism for long-term consequences of TBI. Our MRI-based technique, DCM, enables high sensitivity to subtle changes in BBB permeability.[8] We previously showed in post-ischemic stroke patients that in ∼30% of those with no BBBd according to standard MRI, DCM showed significant volumes of disruption. In those patients showing enhancement on standard MRI, the volume of BBBd depicted in the DCM maps was nearly three times larger, reflecting higher sensitivity to BBBd.[8]

We further showed, in a patient scanned repeatedly up to 18 min post-contrast injection, that Ktrans maps (calculated by fitting the data to a two compartment model) and our BBB maps (calculated by subtracting the early images from the delayed images) showed similar results at different delays post-contrast, suggesting that the increased sensitivity stems from the long delay and not from the method used for calculating the maps. For example, the disruption volumes depicted in the maps calculated at 16 min post-contrast were significantly larger (5.6 ± 1.4 according to the DCE two-compartment model and 5.8 ± 2.2 according to the DCM subtraction method; $p < 0.0001$ for both) than those calculated at 4 min (the standard delay used for DCE).

In the current work, we implemented the DCM methodology to follow short-and long-term changes in BBB function post-TBI in a CHI experimental model. Our DCM methodology was significantly advantageous over standard MRI because of the high sensitivity derived from the relatively long delay (30 min) compared with standard contrast-enhanced T1-MRIs. The BBBd volumes were significantly larger at the acute and the chronic time points in the BBB maps. Moreover, BBBd was undetectable in 33% of T1-MRIs, but was clearly detected at all time points in the BBB maps. In addition, in those cases where BBBd could be detected in T1-MRI, the extent/volumes were significantly larger and appeared more diffuse in the BBB maps. Remarkably, using our DCM longitudinally, the BBB maps showed significant BBBd in the lesioned cortex up to 540 days (1.5 years) after injury (Fig. 2A,2B), suggesting that BBB function never completely recovered after TBI.

These findings were confirmed by comparing the DCM results with different histological analyses that were performed on the same brains. Because we used a clinical 1.5 T scanner, the BBB map resolution (which is identical to the T1-MRI resolution) was significantly lower than that of the histological samples. The ROI we considered as LC in the MRI actually covered both the LC and CG histological regions. The LC and CG (which is located lateral and adjacent to LC), were directly affected by the initial impact to the brain, whereas PC, located medi-

ally and relatively remote from the lesion, was not directly affected by the insult. This is the rationale, when studying the correlation between DCM and histological parameters, for our main focus on the LC and CG regions.

Histological analysis enables evaluation of the extent of BBB damage with high resolution in different brain regions and allows investigation of different BBB components. The BBB is composed of three cellular elements of the brain microvasculature: endothelial cells, astrocyte end-feet, and pericytes. The TJs, which are present between the cerebral endothelial cells, form a barrier that selectively excludes most blood-borne substances from entering the brain. Astrocytic end-feet tightly unsheathe the vessel wall and appear to be critical for the induction and maintenance of the TJs barrier.[1,2]

In our study, three histological assessments were performed, representing different aspects of the blood vessel integrity: the blood vessel coverage parameter, where we stained astrocyte end-feet with GFAP or AQP4, represents the unsheathe of the endothelial cells and thus points to the integrity of the neurovascular unit (NVU). The ZO-1 is a TJ scaffold protein expressed on the microvascular endothelial cells of the BBB, which participates in the strong sealing of gaps between adjacent endothelial cells, thus limiting passage of molecules through the paracellular routes, and is therefore considered a major factor affecting BBB permeability. Accordingly, the percentage of ZO-1 gap parameter represents integrity of the endothelial component of the BBB.[35]

The TJs functional integrity at the BBB can be evaluated by measuring the extravasation of solutes that are not transport substrates and typically remain in the vascular lumen under physiological conditions. It is common knowledge that the levels of endogenous proteins, such as IgG, are highly elevated in the blood after TBI.[37,44] Because IgG is a relatively large molecule (∼150 kDa), however, it does not penetrate the BBB unless the latter's function is compromised. Therefore, the IgG leakage parameter represents BBB malfunction. We found extensive IgG leakage mainly in the ipsilateral hemisphere, affected directly by the insult, in the acute time points (up to 8 days). Later on, extravasation levels were reduced dramatically. As the disruption was subtle in the chronic phase following injury, we could not detect IgG leakage into the brain parenchyma, despite observing other BBBd hallmarks.

Importantly, despite the resolution differences, all the measurements, including DCM, microvessel coverage, number of ZO-1 gaps, and IgG leakage, showed significant BBBd immediately post-injury followed by significant recovery. All measurements (including DCM, microvessel coverage, number of ZO-1 gaps, and IgG leakage), however, showed continuous significant BBBd throughout the follow-up time, without reaching full

recovery. This BBBd was confirmed as significantly higher than that of healthy age-matched controls.

Although sharing same trends, we found some differences in the recovery time lines. DCM showed significant BBBd immediately after the injury, with significant improvement after 8 days, suggesting partial improvement during the acute stage. This improvement during the acute stage was consistent with the AQP-4 microvessel coverage results, but was not detected by the GFAP staining and the number of ZO-1 gaps. In the case of GFAP, this may be explained by the limited sensitivity relative to AQP-4 staining. DCM showed additional significant improvement up to 60 days. This improvement was consistent with both the GFAP and AQP-4 microvessel coverage findings, but inconsistent with the number of ZO-1 gaps, showing later significant improvement between 60 and 540 days. This may suggest that different components of the NVU recovered at different time points.

In summary, our results show that the DCM-based methodology can detect BBB permeability up to 1.5 years after CHI in mice, with significantly higher sensitivity than contrast-enhanced T1-weighted and T2-weighted MRI. The histological findings, presenting different components of the BBB, support the MRI findings and show significant correlations with the parameters obtained from DCM. Further, the histological analysis revealed the extent of BBB damage at the cellular and molecular level.

Regions that are normally considered healthy or intact because they are located away from the injury area, even in the contralateral hemisphere, were found in our study to be abnormal. This was reflected by decreased TJs proteins levels, expressed as an increased percentage of ZO-1 gaps, and decreased BV coverage by astrocyte endfeet even in the contralateral hemisphere far from the impact region. According to the DCM methodology, BBBd measured with MRI paralleled many of the histological results. In addition to the significant correlations found between the MRI findings and the histological parameters, BBBd in remote regions, such as the contralateral LC, were affected, pointing to DCM as a valid and sensitive method for non-invasive assessment of subtle BBBd.

Cumulative evidence from recent years points to BBB integrity as a central component of the pathophysiology of TBI. In addition, changes in BBB integrity is a well documented phenomenon in healthy aging[10,45–47] and was recently suggested as an early biomarker of cognitive dysfunction independent of Aβ and/or tau biomarker changes in patients with Alzheimer disease.[24] Therefore, it is expected that routine use of high-resolution non-invasive techniques to measure BBB integrity, such as DCM with advanced analysis methods, may enhance our understanding of the changes in BBB function after TBI and normal aging.

Revealing these secondary damage mechanisms will lead the way for improved diagnosis and prognosis, enabling determination of early biomarkers for identifying patients at risk for development of late complications such as neurodegenerative diseases. In addition, it may open horizons to novel treatment targets and approaches.

Key limitations: the main limitation of this study is the small sample size, particularly in the histological analysis. The longitudinal analysis of up to 1.5 years after the injury is a significant strength, however. The current study was focused on the application of DCM for longitudinal depiction and quantification of subtle BBBd in a TBI model in an attempt to demonstrate long-term chronic BBB abnormalities. In recent years, there is accumulating evidence suggesting that chronic subtle BBBd may act as a major underlying mechanism of cognitive decline after TBI. The current study, however, does not follow acute or chronic functional outcomes and therefore cannot strengthen or contradict this mechanism.

Further experimental work, which is currently in progress, is essential to address these issues, especially to compare DCM findings to functional outcomes and blood biomarkers.

Transparency, Rigor and Reproducibility Summary

Our paper entitled: Application of delayed contrast extravasation MRI for depicting subtle blood-brain barrier disruption in a TBI model meets the criteria for neuroimaging study. This is the first validation of a new imaging method for depicting long-term subtle BBBd in a CHI model. For this reason, this study was determined as exploratory and was not formally registered. The analysis plan was not formally pre-registered, but the lead authors certify that the analysis plan was pre-specified. To calculate appropriate sample size, *a priori* analysis for a mixed model with post hoc analysis were conducted. Based on our previous results in mice, effect size of 0.4 and a power of 0.95 were chosen, this yielded a total sample size of 24 animals. Since the last time point was planned at 540 days, 1.5 years from injury which considered as old age for rodents, the sample size was increased by 30%. Imaging acquisition and analyses were performed by team members blinded to time point following the injury of the animals, and histological outcomes were assessed by team members blinded to imaging results. All equipment and software used to perform imaging and preprocessing are widely available from commercial sources. All scans were collected using the same MR scanner and the same MR sequences as specified in method section. Image analysis was performed using MATLAB software with a code developed inhouse.[8,48] Characteristics of the primary neuroimaging analyses are described in method section. The time required for image acquisition was 40 minutes, up to

4 mice were scanned together. The time required for generation of each BBB map was approximately 1 minute. Replication by the study group is ongoing and will be registered at Center for Open Science. Analytic codes used to conduct the analyses presented in this study are not available in a public repository. They may be available by emailing the corresponding author. The algorithm is described in detail in the manuscript. This paper will be published under a Creative Commons Open Access license, and upon publication will be freely available at https://www.liebertpub.com/loi/neu.

Acknowledgments

Funding Information

Author Disclosure Statement

No competing financial interests exist.

Supplementary Material

Supplementary Text
Supplementary Table S1

References

1. Lochhead JJ, Yang J, Ronaldson PT, et al. Structure, function, and regulation of the blood-brain barrier tight junction in central nervous system disorders. Front Physiol 2020;11(914); doi:10.3389/fphys.2020.00914
2. Ballabh P, Braun A, Nedergaard M. The blood-brain barrier: an overview: structure, regulation, and clinical implications. Neurobiol Dis 2004;16(1):1–13; doi:10.1016/j.nbd.2003.12.016
3. van Vliet EA, Ndode-Ekane XE, Lehto LJ, et al. Long-lasting blood-brain barrier dysfunction and neuroinflammation after traumatic brain injury. Neurobiol Dis 2020;145(105080); doi:10.1016/j.nbd.2020.105080
4. Friedman A, Kaufer D. Blood-brain barrier in health and disease. Semin Cell Dev Biol 2015;38(1); doi:10.1016/j.semcdb.2015.03.006
5. Li W, Long JA, Watts LT, et al. A quantitative MRI method for imaging blood-brain barrier leakage in experimental traumatic brain injury. PLoS One 2014;9(12):e114173; doi:10.1371/journal.pone.0114173
6. Wang ML, Li WB. Cognitive impairment after traumatic brain injury: The role of MRI and possible pathological basis. J Neurol Sci 2016;370(244–250); doi:10.1016/j.jns.2016.09.049
7. Tofts PS, Kermode AG. Measurement of the blood-brain barrier permeability and leakage space using dynamic MR imaging. 1. Fundamental concepts. Magn Reson Med 1991;17(2):357–367; doi:10.1002/mrm.1910170208
8. Israeli D, Tanne D, Daniels D, et al. The application of MRI for depiction of subtle blood brain barrier disruption in stroke. Int J Biol Sci 2010;7(1):1–8; doi:10.7150/ijbs.7.1
9. Raja R, Rosenberg GA, Caprihan A. MRI measurements of Blood-Brain Barrier function in dementia: A review of recent studies. Neuropharmacology 2018;134(Pt B):259–271; doi:10.1016/j.neuropharm.2017.10.034
10. Verheggen ICM, de Jong JJA, van Boxtel MPJ, et al. Increase in blood-brain barrier leakage in healthy, older adults. Geroscience 2020;42(4):1183–1193; doi:10.1007/s11357-020-00211-2
11. Dickie BR, Parker GJM, Parkes LM. Measuring water exchange across the blood-brain barrier using MRI. Prog Nucl Magn Reson Spectrosc 2020;116(19–39); doi:10.1016/j.pnmrs.2019.09.002
12. Ford JN, Zhang Q, Sweeney EM, et al. Quantitative water permeability mapping of blood-brain-barrier dysfunction in aging. Front Aging Neurosci 2022;14(867452); doi:10.3389/fnagi.2022.867452
13. Chenevert TL, Stegman LD, Taylor JM, et al. Diffusion magnetic resonance imaging: an early surrogate marker of therapeutic efficacy in brain tumors. J Natl Cancer Inst 2000;92(24):2029-–2036; doi:10.1093/jnci/92.24.2029
14. Zach L, Guez D, Last D, et al. Delayed contrast extravasation MRI for depicting tumor and non-tumoral tissues in primary and metastatic brain tumors. PLoS One 2012;7(12):e52008; doi:10.1371/journal.pone.0052008
15. Zach L, Guez D, Last D, et al. Delayed contrast extravasation MRI: a new paradigm in neuro-oncology. Neuro Oncol 2015;17(3):457–465; doi:10.1093/neuonc/nou230
16. Strbian D, Durukan A, Pitkonen M, et al. The blood-brain barrier is continuously open for several weeks following transient focal cerebral ischemia. Neuroscience 2008;153(1):175–181; doi:10.1016/j.neuroscience.2008.02.012
17. Lifshitz J. Experimental CNS trauma: a general overview of neurotrauma research. In: Brain Neurotrauma: Molecular, Neuropsychological, and Rehabilitation Aspects. Kobeissy FH, ed. CRC Press: Boca Raton (FL); 2015.
18. Narayan RK, Michel ME, Ansell B, et al. Clinical trials in head injury. J Neurotrauma 2002;19(5):503–557; doi:10.1089/089771502753754037
19. Bramlett HM, Dietrich WD. Long-term consequences of traumatic brain injury: current status of potential mechanisms of injury and neurological outcomes. J Neurotrauma 2015;32(23):1834–1848; doi:10.1089/neu.2014.3352
20. Mao X, Terpolilli NA, Wehn A, et al. Progressive histopathological damage occurring up to one year after experimental traumatic brain injury is associated with cognitive decline and depression-like behavior. J Neurotrauma 2020;37(11):1331–1341; doi:10.1089/neu.2019.6510
21. Nordstrom P, Michaelsson K, Gustafson Y, et al. Traumatic brain injury and young onset dementia: a nationwide cohort study. Ann Neurol 2014;75(3):374–381
22. Brett BL, Gardner RC, Godbout J, et al. Traumatic brain injury and risk of neurodegenerative disorder. Biol Psychiatry 2022;91(5):498–507; doi:10.1016/j.biopsych.2021.05.025
23. Montagne A, Nation DA, Sagare AP, et al. APOE4 leads to blood-brain barrier dysfunction predicting cognitive decline. Nature 2020;581(7806):71–76; doi:10.1038/s41586-020-2247-3
24. Nation DA, Sweeney MD, Montagne A, et al. Blood-brain barrier breakdown is an early biomarker of human cognitive dysfunction. Nat Med 2019;25(2):270–276; doi:10.1038/s41591-018-0297-y
25. Rodriguez-Grande B, Ichkova A, Lemarchant S, et al. Early to long-term alterations of cns barriers after traumatic brain injury: considerations for drug development. AAPS J 2017;19(6):1615-1625, doi:10.1208/s12248-017-0123-3
26. O'Keeffe E, Kelly E, Liu Y, et al. Dynamic blood-brain barrier regulation in mild traumatic brain injury. J Neurotrauma 2020;37(2):347–356; doi:10.1089/neu.2019.6483
27. Veksler R, Vazana U, Serlin Y, et al. Slow blood-to-brain transport underlies enduring barrier dysfunction in American football players. Brain 2020;143(6):1826–1842; doi:10.1093/brain/awaa140

28. Yu M, Wang M, Yang D, et al. Dynamics of blood brain barrier permeability and tissue microstructure following controlled cortical impact injury in rat: A dynamic contrast-enhanced magnetic resonance imaging and diffusion kurtosis imaging study. Magn Reson Imaging 2019; 62(1-9)– doi:10.1016/j.mri.2019.01.017

29. Chen Y, Constantini S, Trembovler V, et al. An experimental model of closed head injury in mice: pathophysiology, histopathology, and cognitive deficits. J Neurotrauma 1996;13(10):557–568

30. Flierl MA, Stahel PF, Beauchamp KM, et al. Mouse closed head injury model induced by a weight-drop device. Nat Protoc 2009;4(9):1328–1337; doi:10.1038/nprot.2009.148

31. Myronenko A, Song X. Point set registration: coherent point drift. IEEE Trans Pattern Anal Mach Intell 2010;32(12):2262–2275; doi:10.1109/TPAMI.2010.46

32. Myronenko A, Song X. Intensity-based image registration by minimizing residual complexity. IEEE Trans Med Imaging 2010;29(11):1882–1891; doi:10.1109/TMI.2010.2053043

33. Forsythe GE, Malcolm MA, Moler CB. Computer Methods for Mathematical Computations. J Appl Math Mech 1977;59(2):73–144; doi:doi.org/10.1002/zamm.19790590235

34. Brent RP. Algorithms for Minimization without Derivatives. Dover Publications: Prentice-Hall, Englewood Cliffs, New Jersey; 1973

35. Huang J, Li Y, Tang Y, et al. CXCR4 antagonist AMD3100 protects blood-brain barrier integrity and reduces inflammatory response after focal ischemia in mice. Stroke 2013;44(1):190–197; doi:10.1161/STROKEAHA.112.670299

36. Rajkowska G, Hughes J, Stockmeier CA, et al. Coverage of blood vessels by astrocytic endfeet is reduced in major depressive disorder. Biol Psychiatry 2013;73(7):613–621; doi:10.1016/j.biopsych.2012.09.024

37. Ikeshima-Kataoka H, Yasui M. Correlation between astrocyte activity and recovery from blood-brain barrier breakdown caused by brain injury. Neuroreport 2016;27(12):894–900; doi:10.1097/WNR.0000000000000619

38. Price L, Wilson C, Grant G. Blood-brain barrier pathophysiology following traumatic brain injury. In: Translational Research in Traumatic Brain Injury. Laskowitz D, Grant G, eds. CRC Press; Boca Raton (FL); 2016.

39. Hay JR, Johnson VE, Young AM, et al. Blood-brain barrier disruption is an early event that may persist for many years after traumatic brain injury in humans. J Neuropathol Exp Neurol 2015;74(12):1147–1157; doi:10.1097/NEN.0000000000000261

40. Lublinsky S, Major S, Kola V, et al. Early blood-brain barrier dysfunction predicts neurological outcome following aneurysmal subarachnoid hemorrhage. EBioMedicine 2019;43(460-–472); doi:10.1016/j.ebiom.2019.04.054

41. Yoo RE, Choi SH, Oh BM, et al. Quantitative dynamic contrast-enhanced MR imaging shows widespread blood-brain barrier disruption in mild traumatic brain injury patients with post-concussion syndrome. Eur Radiol 2019;29(3):1308–1317; doi:10.1007/s00330-018-5656-z

42. Wei XE, Wang D, Li MH, et al. A useful tool for the initial assessment of blood-brain barrier permeability after traumatic brain injury in rabbits: dynamic contrast-enhanced magnetic resonance imaging. J Trauma 2011;71(6):1645–1650; doi:10.1097/TA.0b013e31823498eb

43. Parker E, Aboghazleh R, Mumby G, et al. Concussion susceptibility is mediated by spreading depolarization-induced neurovascular dysfunction. Brain 2022;145(6):2049–2063; doi:10.1093/brain/awab450

44. Kochis RM, Ahota A, Garcia HB, et al. Modeling the dynamics of a secondary neurodegenerative injury following a mild traumatic brain injury. Annu Int Conf IEEE Eng Med Biol Soc 2021;2021(4469–4472); doi:10.1109/EMBC46164.2021.9629960

45. Moro F, Pischiutta F, Portet A, et al. Ageing is associated with maladaptive immune response and worse outcome after traumatic brain injury. Brain Commun 2022;4(2):fcac036; doi:10.1093/braincomms/fcac036

46. Uprety A, Kang Y, Kim SY. Blood-brain barrier dysfunction as a potential therapeutic target for neurodegenerative disorders. Arch Pharm Res 2021;44(5):487–498; doi:10.1007/s12272-021-01332-8

47. Verheggen ICM, de Jong JJA, van Boxtel MPJ, et al. Imaging the role of blood-brain barrier disruption in normal cognitive ageing. Geroscience 2020;42(6):1751–1764; doi:10.1007/s11357-020-00282-1

48. Sharabi S, Last D, Daniels D, et al. Non-invasive low pulsed electrical fields for inducing bbb disruption in mice-feasibility demonstration. Pharmaceutics 2021;13(2); doi:10.3390/pharmaceutics13020169